Competition among Superconducting, Antiferromagnetic, and Charge Orders with Intervention by Phase Separation in the 2D Holstein-Hubbard Model

Takahiro Ohgoe and Masatoshi Imada
Department of Applied Physics, University of Tokyo, 7-3-1 Hongo, Bunkyo-ku, Tokyo 113-0033, Japan
(Received 16 March 2017; revised manuscript received 25 July 2017; published 8 November 2017)

Using a variational Monte Carlo method, we study the competition of strong electron-electron and electron-phonon interactions in the ground state of the Holstein-Hubbard model on a square lattice. At half filling, an extended intermediate metallic or weakly superconducting (SC) phase emerges, sandwiched between antiferromagnetic and charge order (CO) insulating phases. By carrier doping into the CO insulator, the SC order dramatically increases for strong electron-phonon couplings, but is largely hampered by wide phase separation (PS) regions. Superconductivity is optimized at the border to the PS.

DOI: 10.1103/PhysRevLett.119.197001

Introduction.—The electron-phonon interaction in condensed matter is the origin of many important phenomena, such as conventional superconductivity (SC) and charge density waves. In a class of strongly correlated materials, the interplay between electron correlations and electron-phonon interactions is believed to induce novel phenomena such as the unconventional high-T_c s-wave SC in alkali-doped fullerenes [1–3]. Even for high-T_c cuprates, some experiments [4] and theoretical studies [5–7] have suggested the important role of phonons for a full understanding of the electronic properties, including the SC. However, they are still controversial because the relevance of the electron-phonon interaction addressed in previous theoretical works largely relies on adjustable model parameters introduced in an *ad hoc* fashion. In addition, a computationally accurate framework to study the interplay between the electron correlation and the electron-phonon interaction has not been fully explored. To establish the role of phonons in a wide range of strongly correlated materials including cuprates, we need a flexible method which can accurately treat strong electron-electron and electron-phonon interactions on an equal footing.

For decades, variational Monte Carlo (VMC) methods have been applied to investigate strongly correlated electrons [8–10]. The advantage of these methods is that they do not suffer from the notorious negative-sign problem, whereas their accuracy depends on the assumed variational wave function. However, owing to improved efficient optimization methods, such as the stochastic reconfiguration method [11], their accuracy and flexibility have improved through the introduction of many variational parameters [12–19]. These methods have been recently applied to complicated *ab initio* multiorbital effective Hamiltonians [20–22]. Recently, we have successfully extended the many-variable VMC (mVMC) method to electron-phonon coupled systems [23].

The Holstein-Hubbard model is the simplest model for studying the interplay of electron-electron and electron-phonon interactions. However, the phase diagram and physical properties under these two competing interactions are controversial even for ground states. In one dimension and in the Bethe lattice with infinite coordination, the phase diagrams for the Holstein-Hubbard model have been obtained by the density matrix renormalization group (DMRG) [24–26] and dynamical mean-field theory (DMFT) [27,28], respectively. At half filling, the DMRG studies have reported the existence of an intermediate metallic phase between a Mott insulating phase and a charge-order (CO) phase in the ground-state phase diagram. On the other hand, the DMFT study for zero temperature has not found evidence for the intermediate phase [27]. For square lattices, a finite-temperature quantum Monte Carlo (QMC) study has also suggested the emergence of an intermediate paramagnetic metallic phase between the antiferromagnetic (AF) and CO phases [29,30]. However, such a phase diagram cannot be conclusive in the finite-temperature studies because of the Mermin-Wagner theorem.

Another important open issue is found when carriers are doped into the half-filled system. The DMFT study on the Holstein model has revealed the presence of a coexisting phase of CO and SC which is not prevented by the phase separation (PS) [31]. It is interesting to ask whether the coexistence also exists in two dimensions. The connection between the SC and PS is intriguing and has been discussed in the literature [32,33] for a different context, i.e., of a three-band Hubbard model as a model for the cuprates. Recently, their strong connections were observed in the mVMC studies on the Hubbard model [15] and *ab initio* effective Hamiltonian of electron-doped LaFeAsO [21]. A natural question here is whether a phonon-driven PS also has a connection in the case of the s-wave SC. In this Letter, we study these issues by using the mVMC method.

Model.—The Hamiltonian we consider here is given by

$$\mathcal{H} = -t\sum_{\langle i,j\rangle,\sigma}(c^{\dagger}_{i\sigma}c_{j\sigma} + \text{H.c.}) + U\sum_{i} n_{i\uparrow}n_{i\downarrow} + g\sum_{i} x_i n_i + \sum_{i}\left(\frac{p_i^2}{2M} + \frac{M\Omega^2 x_i^2}{2}\right), \quad (1)$$

where t, U, g, and Ω represent the hopping amplitude, the on-site interaction strength between electrons, the electron-phonon interaction strength, and the phonon frequency, respectively. $c_{i\sigma}$ ($c^{\dagger}_{i\sigma}$) represents the annihilation (creation) operator of an electron with spin σ ($=\uparrow$ or $\downarrow$) at the site i. The particle number operators $n_{i\sigma}$ and n_i are defined by $n_{i\sigma} = c^{\dagger}_{i\sigma}c_{i\sigma}$ and $n_i = n_{i\uparrow} + n_{i\downarrow}$. x_i and p_i are the lattice displacement operator and its conjugate momentum operator, respectively. x_i relates to the annihilation (creation) boson (phonon) operator $b_i(b^{\dagger}_i)$ as $x_i = \sqrt{(1/2M\Omega)}(b_i + b^{\dagger}_i)$. The dimensionless electron-phonon interaction strength λ is defined as the ratio of the lattice deformation energy to half the bandwidth $W/2 = 4t$, and we obtain $\lambda = g^2/(M\Omega^2 W)$, where M is the mass of single-component nuclei. If we consider the path-integral representation of the partition function and integrate out the phonon degrees of freedom, the model is exactly mapped onto the Hubbard model with the effective dynamical on-site interaction $U_{\text{eff}}(\omega) = U - \lambda W/[1 - (\omega/\Omega)^2]$. In this Letter, we set $M = t = 1$ as the unit of mass and energy. We consider $N = L^2$ systems on the square lattice with N_e electrons and impose the periodic (antiperiodic) boundary condition in the x (y) direction to satisfy the closed-shell condition. The filling factor and doping (hole) concentration are given by $\rho = N_e/N$ and $\delta = 1 - \rho$, respectively.

Method.—Our variational wave function takes the following form: $|\psi\rangle = \mathcal{P}^{\text{el-ph}}(|\psi^{\text{el}}\rangle|\psi^{\text{ph}}\rangle)$ [23]. Here, $|\psi^{\text{el}}\rangle$ and $|\psi^{\text{ph}}\rangle$ represent variational wave functions for electrons and phonons, respectively. $\mathcal{P}^{\text{el-ph}}$ is the correlation factor that takes into account the entanglement between electrons and phonons. Its explicit form is given by $\mathcal{P}^{\text{el-ph}} = \exp(\sum_{i,j}\alpha_{ij}x_i n_j)$, where α_{ij} are variational parameters.

As $|\psi^{\text{el}}\rangle$, we adopt the generalized pairing wave function with the Gutzwiller [34] and Jastrow correlation factors [35]: $|\psi^{\text{el}}\rangle = \mathcal{P}^{\text{J}}\mathcal{P}^{\text{G}}|\phi^{\text{pair}}\rangle$. The generalized pairing wave function takes the form of $|\phi^{\text{pair}}\rangle = (\sum_{i,j=1}^{N} f_{ij}c^{\dagger}_{i\uparrow}c^{\dagger}_{j\downarrow})^{N_e/2}|0\rangle$, where f_{ij} are variational parameters. This is a generalization of the Hartree-Fock-Bogoliubov–type wave function with AF, CO, or SC orders [13,36] and, thus, flexibly describes these states as well as paramagnetic metals (PMs). In order to reduce the number of independent variational parameters, we assume that f_{ij} have a sublattice structure such that f_{ij} depend on the relative vector $\boldsymbol{r}_i - \boldsymbol{r}_j$ and a sublattice index of the site i which we denote as $\eta(i)$. Thus, $f_{ij} = f_{\eta(i)}(\boldsymbol{r}_i - \boldsymbol{r}_j)$. In the present study, we assume a 2×2 sublattice structure and the number of independent f_{ij} reduces from N^2 to $2 \times 2 \times N$. We also assume a translational symmetry for variational parameters in the correlation factors.

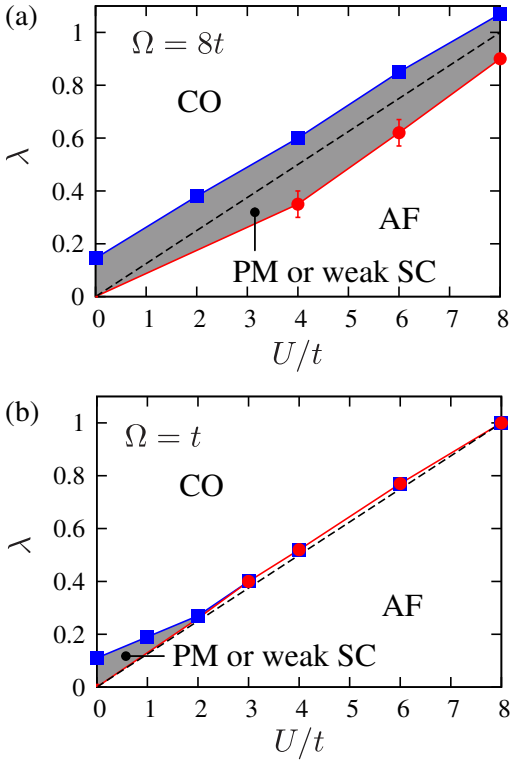

FIG. 1. Ground-state phase diagram of the half-filled Holstein-Hubbard model on a square lattice at (a) $\Omega = 8t$ and (b) $\Omega = t$. The blue squares and red circles represent the boundaries of CO and AF, respectively. Error bars are drawn, but most of them are smaller than the symbol size. Solid lines are used to guide the eye. Dashed lines represent $\lambda = U/8t$. Based on the fact that if $\lambda = 0$, the system is an AF insulator for any $U > 0$ [37], we put the starting point of the AF boundary at the origin. The shaded region represents the intermediate PM or weak SC phase.

For $|\psi^{\text{ph}}\rangle$, we use the tensor product of phonon wave functions with wave vectors $\boldsymbol{q}$: $|\psi^{\text{ph}}\rangle = \prod_{\boldsymbol{q}}|\psi^{\text{ph}}_{\boldsymbol{q}}\rangle$. $|\psi^{\text{ph}}_{\boldsymbol{q}}\rangle$ is expanded in terms of phonon Fock states $|m_{\boldsymbol{q}}\rangle$ as $|\psi^{\text{ph}}_{\boldsymbol{q}}\rangle = \sum_{m_{\boldsymbol{q}}=0}^{m^{\max}_{\boldsymbol{q}}} c_{m_{\boldsymbol{q}}}|m_{\boldsymbol{q}}\rangle$. Here, $m^{\max}_{\boldsymbol{q}}$ are controllable cutoffs for the number of phonons and $c_{m_{\boldsymbol{q}}}$ are treated as variational parameters of real numbers. The number of variational parameters is $\sum_{\boldsymbol{q}}(m^{\max}_{\boldsymbol{q}} + 1)$, which is equal to $N(m^{\max} + 1)$ if we take $m^{\max}_{\boldsymbol{q}} = m^{\max}$. In this study, we checked the convergence of physical quantities as a function of the cutoff and we typically took $m^{\max}_{\boldsymbol{q}} =$ 10–40 for $\boldsymbol{q} = (\pi, \pi)$ and $m^{\max}_{\boldsymbol{q}} = 5$ for others. As initial states in the optimization of variational parameters, we considered the noninteracting Fermi sea (PM state), SC, AF, CO, and coexisting states of SC + AF and SC + CO.

Half-filled case.—We consider two phonon frequencies, an intermediate frequency $\Omega = 8t$ (equal to the bandwidth W) and a smaller one $\Omega = t$. In Fig. 1, we summarize our

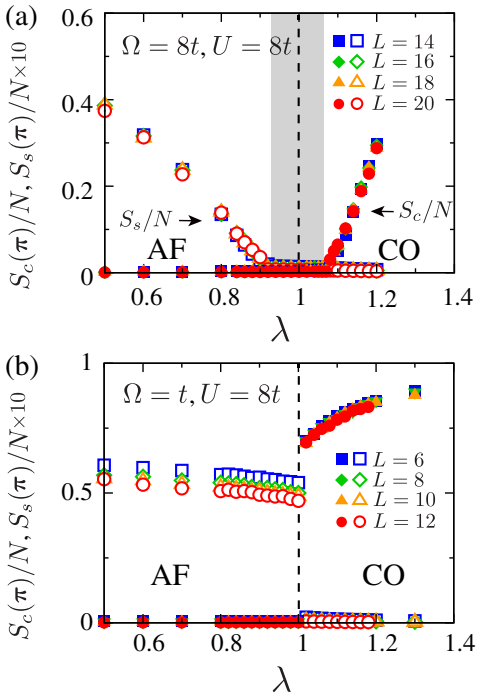

FIG. 2. $S_s(\pi,\pi)/N$ and $S_c(\pi,\pi)/N$ as functions of λ at (a) $(\Omega/t, U/t) = (8,8)$ and (b) $(\Omega/t, U/t) = (1,8)$, respectively. The vertical dashed line represents $U_{\rm eff} = 0$. The shaded region indicates the intermediate metallic (weakly SC) phase.

results in the ground-state phase diagram in the U-λ plane. The phase diagram includes the boundary of the AF and CO phases. To distinguish each phase, we measured the spin structure factor $S_s(\boldsymbol{q}) = (1/3N)\sum_{i,j}\langle \boldsymbol{S}_i \cdot \boldsymbol{S}_j\rangle e^{i\boldsymbol{q}\cdot(\boldsymbol{r}_i-\boldsymbol{r}_j)}$ and the charge structure factor $S_c(\boldsymbol{q}) = (1/N)\sum_{i,j}(\langle n_i n_j\rangle - \rho^2)e^{i\boldsymbol{q}\cdot(\boldsymbol{r}_i-\boldsymbol{r}_j)}$.

One of the main findings in this Letter is the existence of an intermediate phase sandwiched by the AF and CO phases around $U \sim \lambda W$. For $\Omega = 8t$, we found a wide intermediate phase. For the smaller frequency $\Omega = t$, this phase is narrowed but still exists for $U \lesssim 2$. The shrinkage of the intermediate region for small Ω was also observed in one [24,25] and infinite [28] dimensions. Previous QMC studies suggested the intermediate region at $U = 5t$ [29,30]. However, the wider intermediate region in those studies is probably because their calculation is at finite temperature $T/t = 0.25$.

In Figs. 2(a) and 2(b), we plot the spin or charge structure factor $S_{s/c}(\pi,\pi)/N$ as a function of λ at $(\Omega/t, U/t) = (8,8)$ and $(\Omega/t, U/t) = (1,8)$, respectively. In the intermediate region, the values of $S_{s/c}(\pi,\pi)/N$ vanish after its extrapolation to the thermodynamic limit (see Supplemental Material [38] for the extrapolation procedure). The presence of the intermediate phase is further evidenced by the two first-order transitions signaled by two energy-level crossings as a function of λ, where the AF phase energy crosses with the intermediate phase energy at

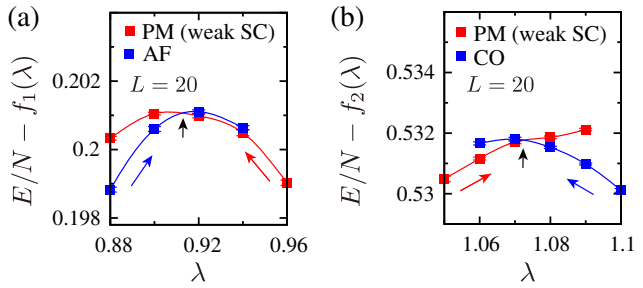

FIG. 3. $E/N - \lambda$ curves of PM (weak SC) states crossing with (a) AF and (b) CO states at $(\rho, \Omega/t, U/t) = (1,8,8)$. The paths are along the vertical line at $U/t = 8$ at the top right of Fig. 1(a). The curves are obtained by gradually changing λ (in the direction indicated as colored arrows). Unimportant linear terms $f_1(\lambda)$ and $f_2(\lambda) \propto \lambda$ are subtracted from E/N for clarity. The crossing points are indicated as black arrows.

$\lambda \sim 0.91$, as shown in Fig. 3(a), and then the latter crosses with the CO phase slightly above $\lambda \sim 1.07$, as in Fig. 3(b), with increasing λ at fixed U and Ω. One may infer that the antiadiabatic or the adiabatic limits may further give useful insights. These are examined in Supplemental Material [38]. In the intermediate region, it is likely that weak SC orders emerge, while expected amplitudes of the order are too weak; thus, we could not distinguish them from PM states in the available data of finite systems (see Supplemental Material [38]).

Doped case.—We now study the doped region. In Fig. 4, we first present our ground-state phase diagram at $U = 0$ in the δ-λ plane for $\Omega = 8t$ and $\Omega = t$, because the $U = 0$ phase diagram captures an essential aspect. For $U = 0$, the effective interaction $U_{\rm eff}(\omega)$ has negative parts for $\omega < \Omega$, which lead to s-wave SC states except for the gapped CO phase at half filling. In our phase diagram, the SC + CO phase is absent. Instead, the PS region appears adjacent to the CO phase at half filling. We find that for the smaller phonon frequency, the PS region is enlarged. In the Supplemental Material [38], we present the phase diagram in the adiabatic limit as the extreme case. In Fig. 4, we also plot $S_c(\pi,\pi)/N$ and the long-range part of the s-wave SC correlation function P_s^∞, which is defined by $P_s^\infty = (1/M)\sum_{\sqrt{2}L/4<|\boldsymbol{r}|} P_s(\boldsymbol{r})$. Here, $\boldsymbol{r}$ is the relative position vectors belonging to $(-L/2, L/2]^2$, M is the number of vectors satisfying $\sqrt{2}L/4 < |\boldsymbol{r}| < \sqrt{2}L/2$, and the SC function $P_s(\boldsymbol{r})$ is defined by $P_s(\boldsymbol{r}) = (1/N)\sum_{\boldsymbol{r}_i}\langle \Delta_s^\dagger(\boldsymbol{r}_i)\Delta_s(\boldsymbol{r}_i+\boldsymbol{r})\rangle$ with the order parameter $\Delta_s(\boldsymbol{r}_i) = c_{\boldsymbol{r}_i\uparrow}c_{\boldsymbol{r}_i\downarrow}$.

In Fig. 5(a), we show physical quantities which were used to determine the phase diagrams in Fig. 4 in an example at $(\Omega/t, U/t, \lambda) = (8,0,0.3)$. We also show an interacting case for $(\Omega/t, U/t, \lambda) = (8,8,1.3)$ in Fig. 5(b) for comparison. Since the model is mapped, in the antiadiabatic limit, to the standard Hubbard model with the on-site interaction $U_{\rm eff} = U - W\lambda$, the comparison between the interacting and noninteracting cases with the same $U_{\rm eff}$ may provide us with insight for large Ω. The cases shown in

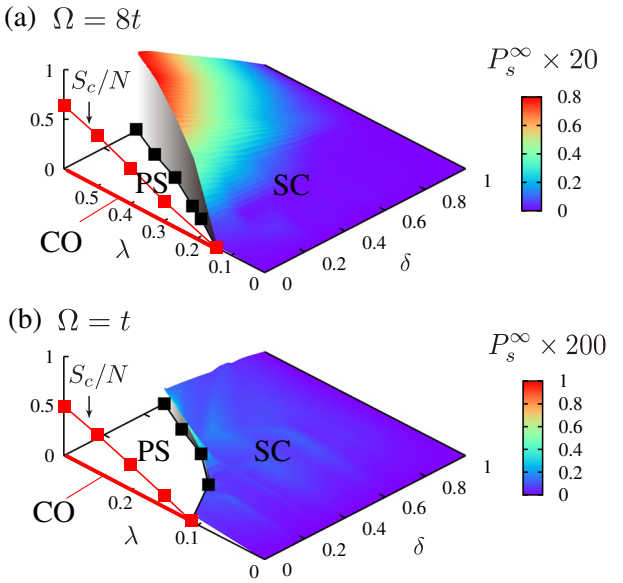

FIG. 4. Ground-state phase diagrams of the Holstein model in the δ-λ plane at (a) $\Omega = 8t$ and (b) $\Omega = t$. In the vertical axis, $S_c(\pi,\pi)/N$ (red squares) and P_s^∞ (color plots) for $L = 14$ are plotted in the CO and SC phases, respectively. Black squares in the bottom plane represent boundaries between the PS and s-wave SC regions. White areas denote the PS regions. Thick red lines at $\delta = 0$ indicate the CO phase.

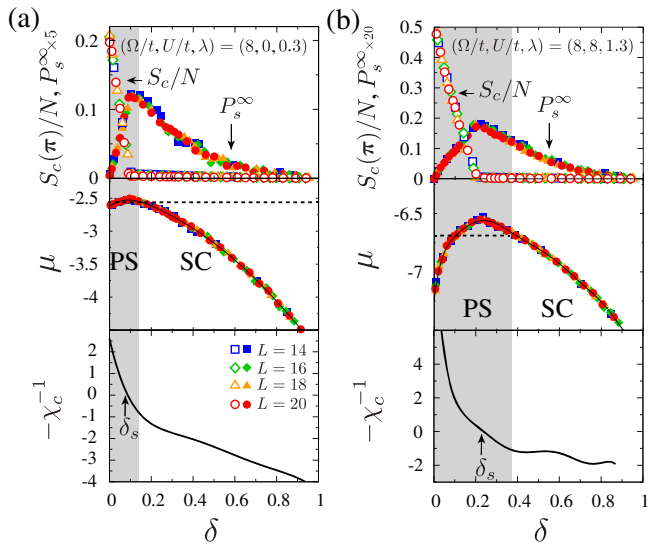

FIG. 5. Physical quantities $S_c(\pi,\pi)/N$, P_s^∞, μ, and $-\chi_c^{-1}$ as functions of doping δ at (a) $(\Omega/t, U/t, \lambda) = (8, 0, 0.3)$ and (b) (8, 8, 1.3), respectively. The shaded area denotes the PS region, which was determined by the Maxwell construction. The dashed horizontal line in the middle panel is used for the Maxwell construction. The curves of $-\chi_c^{-1}$ were derived from the derivative of the $\mu - \delta$ curves (black curves) which were obtained by the seventh-order polynomial fit. The spinodal points δ_s are indicated as the arrows.

Figs. 5(a) and 5(b) indeed have the same $U_{\rm eff} = -2.4$. The value of $S_c(\pi,\pi)/N$ decreases monotonically and the CO eventually disappears at $\delta \simeq 0.1$ and 0.2 for $U/t = 0$ [Fig. 5(a)] and $U/t = 8$ [Fig. 5(b)], respectively. On the other hand, the value of P_s^∞ increases as δ increases and we clearly observe the SC phase. For small δ, a CO order and an s-wave SC order coexist. By the Maxwell construction for the δ-μ curve, however, we find that the SC + CO phase is swallowed up by the PS region ($0 < \delta < 0.14$ for $U/t = 0$ and $0 < \delta < 0.37$ for $U/t = 8$). Here, μ is the chemical potential which was calculated by $\mu(\bar{N}_e) = [E(N_e) - E(N_e')]/(N_e - N_e')$. Here, E is the total energy, (N_e, N_e') are the electron numbers, and we obtain the chemical potential at the mid filling $\bar{N}_e = (N_e + N_e')/2$. Our Hamiltonian has the particle-hole symmetry at $\mu = -8\lambda - U/2 = -2.4$ and -6.4 for Figs. 5(a) and 5(b), respectively. Since this value is above the line used for the Maxwell construction, there is a charge gap at half filling. For the interacting case Fig. 5(b), the charge gap is even larger. We also present the negative inverse uniform charge susceptibility $-\chi_c^{-1} = d\mu/d\rho$ in Fig. 5. In our model, the spinodal point δ_s, where the uniform charge susceptibility diverges ($\chi_c^{-1} = 0$), coincides with the critical point of the CO and, therefore, the PS is driven by the CO (see also the results for the adiabatic limit in the Supplemental Material [38]).

Comparisons between Figs. 5(a) and 5(b) show a quantitative difference that the CO (SC) orders are enhanced (suppressed) for large U/t. However, we find a universal common feature both in Figs. 5(a) and 5(b); a clear one-to-one correspondence among the peak of the SC order, the spinodal point, and the border of the CO phase thus indicates tight connections of the mechanism of the SC, CO, and uniform charge instability. The strong effective attractive interaction of carriers is certainly the key, because it causes all of these three properties. The strong attraction is caused by the electron-phonon interaction here, while the resultant charge fluctuations may also work as additional glue of the Cooper pair. The same trend between the enhancement of the s-wave SC and the uniform charge susceptibility has been reported for d-wave SC in the Hubbard model [15] and extended s-wave SC in the *ab initio* effective Hamiltonian for LaFeAsO [21] as well.

To summarize, by studying the ground states of the Holstein-Hubbard model on a square lattice, we have clarified where the s-wave SC is enhanced in the phase diagram. At half filling, we have found an intermediate metallic or weakly SC region sandwiched by the CO and AF phases. In the doped case, the SC is dramatically enhanced, but a wide PS region triggered by the CO largely hinders the SC and completely preempts the SC + CO phase. We have revealed that the SC is optimized at the border of the PS. These findings have been obtained by the VMC method extended for electron-phonon coupled systems. Our method is quite flexible, and therefore it will be also useful to study more complicated systems such as *ab initio* Hamiltonians of high-T_c cuprates, where several different phonon modes are present.

We thank Kota Ido for useful discussions. T. O. also thanks Yuta Murakami for discussions. The code was developed based on the open-source software mVMC [48]. This work is financially supported by the Ministry of Education, Culture, Sports, Science and Technology (MEXT) High Performance Computing Infrastructure (HPCI) Strategic Programs for Innovative Research (SPIRE), the Computational Materials Science Initiative (CMSI), and Creation of New Functional Devices and High-Performance Materials to Support Next Generation Industries (CDMSI). This work was also supported by a Grant-in-Aid for Scientific Research (Grants No. 22104010, No. 22340090, and No. 16H06345) from MEXT, Japan. The simulations were partially performed on the K computer provided by the RIKEN Advanced Institute for Computational Science under the HPCI System Research project (Projects No. hp130007, No. hp140215, No. hp150211, No. hp160201, and No. hp170263). The simulations were also performed on computers at the Supercomputer Center, Institute for Solid State Physics, University of Tokyo.

[1] A. Y. Ganin, Y. Takabayashi, P. Jeglič, D. Arčon, A. Potočnik, P. J. Baker, Y. Ohishi, M. T. McDonald, M. D. Tzirakis, A. McLennan *et al.*, Nature (London) **466**, 221 (2010).
[2] M. Capone, M. Fabrizio, C. Castellani, and E. Tosatti, Science **296**, 2364 (2002).
[3] Y. Nomura, S. Sakai, M. Capone, and R. Arita, Sci. Adv. **1**, e1500568 (2015).
[4] A. Lanzara, P. V. Pogdanov, X. J. Zhou, S. A. Kellar, D. L. Feng, E. D. Lu, T. Yoshida, H. Eisaki, A. Fujimori, K. Kishio *et al.*, Nature (London) **412**, 510 (2001).
[5] Z. B. Huang, W. Hanke, E. Arrigoni, and D. J. Scalapino, Phys. Rev. B **68**, 220507(R) (2003).
[6] S. Ishihara and N. Nagaosa, Phys. Rev. B **69**, 144520 (2004).
[7] S. Johnston, I. M. Vishik, W. S. Lee, F. Schmitt, S. Uchida, K. Fujita, S. Ishida, N. Nagaosa, Z. X. Shen, and T. P. Devereaux, Phys. Rev. Lett. **108**, 166404 (2012).
[8] D. Ceperley, G. V. Chester, and M. H. Kalos, Phys. Rev. B **16**, 3081 (1977).
[9] H. Yokoyama and H. Shiba, J. Phys. Soc. Jpn. **80**, 084607 (2011).
[10] M. Capello, F. Becca, M. Fabrizio, S. Sorella, and E. Tosatti, Phys. Rev. Lett. **94**, 026406 (2005).
[11] S. Sorella, Phys. Rev. B **64**, 024512 (2001).
[12] S. Sorella, Phys. Rev. B **71**, 241103(R) (2005).
[13] D. Tahara and M. Imada, J. Phys. Soc. Jpn. **77**, 114701 (2008).
[14] R. Kaneko, S. Morita, and M. Imada, J. Phys. Soc. Jpn. **83**, 093707 (2014).
[15] T. Misawa and M. Imada, Phys. Rev. B **90**, 115137 (2014).
[16] S. Morita, R. Kaneko, and M. Imada, J. Phys. Soc. Jpn. **84**, 024720 (2015).
[17] M. Kurita, Y. Yamaji, S. Morita, and M. Imada, Phys. Rev. B **92**, 035122 (2015).
[18] L. F. Tocchio, F. Becca, A. Parola, and S. Sorella, Phys. Rev. B **78**, 041101 (2008).
[19] L. F. Tocchio, F. Becca, and C. Gros, Phys. Rev. B **83**, 195138 (2011).
[20] H. Shinaoka, T. Misawa, K. Nakamura, and M. Imada, J. Phys. Soc. Jpn. **81**, 034701 (2012).
[21] T. Misawa and M. Imada, Nat. Commun. **5**, 5738 (2014).
[22] M. Hirayama, T. Misawa, T. Miyake, and M. Imada, J. Phys. Soc. Jpn. **84**, 093703 (2015).
[23] T. Ohgoe and M. Imada, Phys. Rev. B **89**, 195139 (2014).
[24] R. T. Clay and R. P. Hardikar, Phys. Rev. Lett. **95**, 096401 (2005).
[25] M. Tezuka, R. Arita, and H. Aoki, Phys. Rev. B **76**, 155114 (2007).
[26] H. Fehske, G. Hager, and E. Jeckelmann, Europhys. Lett. **84**, 57001 (2008).
[27] J. Bauer and A. C. Hewson, Phys. Rev. B **81**, 235113 (2010).
[28] Y. Murakami, P. Werner, N. Tsuji, and H. Aoki, Phys. Rev. B **88**, 125126 (2013).
[29] E. A. Nowadnick, S. Johnston, B. Moritz, R. T. Scalettar, and T. P. Devereaux, Phys. Rev. Lett. **109**, 246404 (2012).
[30] S. Johnston, E. A. Nowadnick, Y. F. Kung, B. Moritz, R. T. Scalettar, and T. P. Devereaux, Phys. Rev. B **87**, 235133 (2013).
[31] Y. Murakami, P. Werner, N. Tsuji, and H. Aoki, Phys. Rev. Lett. **113**, 266404 (2014).
[32] M. Grilli, R. Raimondi, C. Castellani, C. Di Castro, and G. Kotliar, Phys. Rev. Lett. **67**, 259 (1991).
[33] R. Raimondi, C. Castellani, M. Grilli, Y. Bang, and G. Kotliar, Phys. Rev. B **47**, 3331 (1993).
[34] M. C. Gutzwiller, Phys. Rev. Lett. **10**, 159 (1963).
[35] R. Jastrow, Phys. Rev. **98**, 1479 (1955).
[36] T. Giamarchi and C. Lhuillier, Phys. Rev. B **43**, 12943 (1991).
[37] J. E. Hirsch, Phys. Rev. B **31**, 4403 (1985).
[38] See Supplemental Material at http://link.aps.org/supplemental/10.1103/PhysRevLett.119.197001 for a detailed analysis of the extrapolation of the structure factors to the thermodynamic limit, the superconducting correlation functions at half filling, the physical properties in the antiadiabatic or adiabatic regime, and a possible incommensurate order; this includes Refs. [39–47].
[39] D. A. Huse, Phys. Rev. B **37**, 2380(R) (1988).
[40] D. Hurt, E. Odabashian, W. E. Pickett, R. T. Scalettar, F. Mondaini, T. Paiva, and R. R. dos Santos, Phys. Rev. B **72**, 144513 (2005).
[41] C. N. Varney, C.-R. Lee, Z. J. Bai, S. Chiesa, M. Jarrell, and R. T. Scalettar, Phys. Rev. B **80**, 075116 (2009).
[42] N. Furukawa and M. Imada, J. Phys. Soc. Jpn. **61**, 3331 (1992).
[43] A. W. Sandvik, Phys. Rev. B **56**, 11678 (1997).
[44] K. Dichtel, R. J. Jelitto, and H. Koppe, Z. Phys. **246**, 248 (1971).
[45] H. Shiba, Prog. Theor. Phys. **48**, 2171 (1972).
[46] A. Moreo and D. J. Scalapino, Phys. Rev. Lett. **66**, 946 (1991).
[47] M. Vekić, R. M. Noack, and S. R. White, Phys. Rev. B **46**, 271 (1992).
[48] https://github.com/issp-center-dev/mVMC.